Improving Predictions of Spin-Crossover Complex Properties through DFT Calculations with a Local Hybrid Functional

Citation: Improving Predictions of Spin-Crossover Complex Properties through DFT Calculations with a Local Hybrid Functional. Sangeeta Rajpurohit, Vyshnavi Vennelakanti, and Heather J. Kulik. The Journal of Physical Chemistry. A 2024 128 (41), 9082-9089

Published Version: 10.1021/acs.jpca.4c05046

Publisher: American Chemical Society

Permanent Link: https://hdl.handle.net/1721.1/162786

Version: Author's final manuscript: final author's manuscript post peer review, without publisher's formatting or copy editing

Improving Predictions of Spin-Crossover Complex Properties through DFT Calculations with a Local Hybrid Functional

Sangeeta Rajpurohit,[†] Vyshnavi Vennelakanti,[‡,¶] and Heather J. Kulik[‡,¶]

†*Molecular Foundry, Lawrence Berkeley National Laboratory, USA*

‡*Department of Chemical Engineering, Massachusetts Institute of Technology, Cambridge, Massachusetts, USA*

¶*Department of Chemistry, Massachusetts Institute of Technology, Cambridge, Massachusetts, USA*

E-mail:

Abstract

We conducted a study on the performance of the local hybrid exchange-correlation functional PBE0r for a set of 95 experimentally-characterized iron spin crossover (SCO) complexes [V. Vennelakanti et al., J. Chem. Phys. (2023)]. The PBE0r functional is a variant of PBE0 where the exchange correction is restricted to on-site terms formulated within the basis of local orbitals. We determine the free parameters of the PBE0r functional against experimental data and other hybrid functionals. With a Hartree-Fock (HF) exchange factor of 4%, the PBE0r functional accurately reproduces the electronic and free energy trends predicted in prior DFT studies for these 95 complexes using the B3LYP functional. Larger values of HF exchange stabilize high-spin states. The PBE0r-predicted bond lengths tend to exceed the experimental bond lengths, and bond lengths are less sensitive to HF exchange. The predicted SCO transition temperatures

$T_{1/2}$ from PBE0r correlate moderately with the experimental transition temperatures, showing a slight improvement compared to the previous modB3LYP-predicted $T_{1/2}$. This study suggests the PBE0r functional as computationally cost-effective and offers the possibility of simulating larger complexes with accuracy comparable to other global hybrid functionals, provided the HF exchange parameter is carefully optimized.

Introduction

Spin crossover (SCO), which is the change in spin multiplicity under the influence of external perturbation, represents one of the most interesting phenomena in the field of coordination chemistry due to its wide application, including optical switches and memory devices.[1–4] This phenomenon predominantly manifests in compounds containing metals with electronic configurations ranging from d^4 to d^7. Mononuclear iron(II) complexes are among these extensively studied SCO molecular systems.[4,5] In octahedral Fe(II) complexes with a d^6 configuration, SCO can be induced thermally, optically, or by varying pressure, leading to transitions between the high-spin ($^5T_2$) and low-spin ($^1A_1$) states, accompanied by notable structural changes. The accurate description of energy differences between different spin states is crucial for the correct prediction of SCO phenomena, particularly in the context of new information processing devices.

Advanced electronic structure methods are necessary to accurately model Fe(II) complexes, particularly when assessing the energetics of the spin states. Among these approaches, two widely used wave-function-based methods are single-reference methods like CCSD(T)[6] and multi-reference methods such as CASPT2.[7,8] CCSD(T) and CASPT2 are considered reliable methods to obtain reference data for benchmarking other theoretical methods. However, notable discrepancies between CCSD(T) and CASPT2 have also been reported,[9,10] highlight potential limitations when using these methods for generating reference data. CCSD(T) is inadequate in providing accurate descriptions for systems with strong multiconfigurational character, including Fe(II) complexes in their low-spin (LS) states. Moreover, the very high

computational cost of calculations, which scale as $O(N^7)$ with system size, in CCSD(T) restricts its applicability to complexes comprising only a few tens of atoms. Computationally feasible variants of CCSD(T) method, such as domain-based local pair natural orbital (DLPNO-CCSD(T)) approach,[11–14,14–16] for studying medium- and large-sized complexes have been developed. Several CASPT2 studies reveal a systematic bias towards high-spin (HS) states largely attributed to an inadequate treatment of outer-core 3s3p correlation effects, when compared to reference data calculated with CCSD(T).[10,17,18] To overcome this bias of CASTP2 towards HS states, Phung et al. proposed a combined CASPT2/CC approach, which involves treating correlations of valence electrons with CASPT2 with a larger basis set and semi-core correlation with CCSD(T).[19]

Single-reference methods based on density functional theory (DFT), where static and dynamic correlation effects are partially incorporated, provide computationally effective alternatives to multiconfigurational methods for studying large SCO systems. While DFT-predicted complex geometries and structural properties are very accurate, the energetics of spin-states are strongly dependent on the exchange-correlation functionals. There has been extensive discussion in the literature regarding the choice of the most appropriate XC functional for describing SCO complexes, with no complete consensus has been reached thus far. Ab-initio Hartree-Fock theory (HF)[20] tends to show a preference for the HS state, while pure DFT functionals typically favor the LS state. The semi-local XC functional GGA and meta-GGA consistently overestimate the stability of the LS states.[21–23] A middle ground is reached using hybrid DFT functionals, which incorporate a fraction of HF exchange. In general, the global hybrid and range-separated functionals perform better than GGA and meta-GGA.[23–25] However, ideal parameter selection remains a major concern for hybrid functionals. Several previous studies consistently show that the accurate prediction of the ground state requires a small proportion, often as small as $10-15\%$, of exact-exchange in global hybrids and short-range exchange within range-separated hybrids.[23,26] While several past studies have evaluated the appropriateness of this HF exact exchange choice in small

iron-based model systems,[23,26,27] comprehensive examinations on larger complexes featuring diverse ligands and varying ligand-field strengths are warranted.

A recent study on $[Fe^{II}(NH_3)_6]^{2+}$ by Römer et al.[23] benchmarked global hybrid PBE0[28] and B3LYP,[29] the range-separated hybrid CAM-B3LYP,[30] and the recently proposed local hybrid functional PBE0r[31] against reference values for spin-splitting energies calculated with correlated coupled-cluster calculations. The study shows a good agreement between the recently proposed PBE0r and CCSD(T). However, the performance of the PBE0r functional against the large experimental data set remains to be tested. Within local PBE0r functional, the wave functions represented in augmented waves are mapped onto a basis set of local orbitals. The long-range screening of the Coulomb interaction is achieved by only including exchange terms in the basis set of these local orbitals while excluding off-site terms, significantly reducing computational costs. In this work, we test the predictive capabilities of the above local hybrid functional PBE0r by studying a comprehensive dataset comprising 95 Fe(II) complexes from reference;[26] from now on we refer to it as SCO-95. We determined a parameter range for the free parameter in the PBE0r functional to accurately describe the spin-splitting energies, geometries and SCO transition temperatures $T_{1/2}$ of these complexes.

Methods

The PBE0r hybrid functional[31–33] is a range-separated variant of the global PBE0 hybrid functional.[28] The PBE0r functional restricts exact exchange contributions to on-site terms, whereas the long-range inter-site exchange contributions are treated within the density functional approximation. The exchange-correlation energy E_{XC}^{PBE0r} in the PBE0r functional is given by

$$E_{XC}^{PBE0r} = E_{XC}^{PBE} + \sum_R \alpha_R (E_{X,R}^{HF} - E_{X,R}^{DC}) \tag{1}$$

where E_{XC}^{PBE} is the PBE functional[34] and $E_{X,R}^{HF}$ is the on-site Hartree-Fock exchange energy for site R. $E_{X,R}^{DC}$ is a double-counting correction, which subtracts exchange contributions that are taken into account by both $E_{X,R}^{HF}$ and E_{XC}^{PBE}. The HF mixing strength is controlled for each site R by the factor α_R. The on-site HF exchange terms $E_{X,R}^{HF}$, which include both the valence-valence as well as the valence-core exchange interactions, and the double count correction $E_{X,R}^{DC}$ are computed on an atom-centered tight-binding orbital basis. The Kohn-Sham orbitals are mapped onto this atom-centered tight-binding orbital basis. A set of local orbitals $\{\chi_R\}$ is constructed for every atomic site R. The local orbitals are atom-centered Hankel functions, that are augmented at their center by partial waves after including one scattering wave to the partial wave set.[35] Each orbital $|\chi_{R_a}\rangle$ localized at the atom R has a corresponding local orbital projector $|\tilde{\pi}_{R_a}\rangle$. These local orbital projector functions $|\tilde{\pi}_{R_a}\rangle$ are constructed carefully to minimize the deviation of the state

$$|\psi_n'\rangle = \sum_R \sum_{a\in R} |\chi_{R_a}\rangle\langle\tilde{\pi}_{R_a}|\psi_n\rangle \tag{2}$$

from the KS state $|\psi_n\rangle$. The HF exchange energy $E_{X,R}^{HF}$ for atom R is expressed as

$$E_{X,R}^{HF} = -\frac{1}{2}\sum_{abcd\in R} \rho_{R,cd} U_{R,dabc} \rho_{R,ba} \tag{3}$$

where the local Coulomb tensor elements $U_{R,dabc}$ for site R are computed by using the Laplace multipole expansion of the Coulomb interaction. Here, the elements of the one-particle density matrix $\rho_{R,ab}$ are defined as

$$\rho_{R,ab} = \sum_n f_n \langle\tilde{\pi}_{R_a}|\psi_n\rangle\langle\psi_n|\tilde{\pi}_{R_b}\rangle \tag{4}$$

are obtained by projecting the occupancies f_n of the KS wavefunctions $|\psi_n\rangle$ onto the local

orbitals. The double-counting correction term

$$E_{X,R}^{DC} = \sum_{R} \int d^3\vec{r} \frac{n_R(\vec{r})}{n(\vec{r})} n_R(\vec{r}) \epsilon_{xc}(\vec{r}), \tag{5}$$

where, $\epsilon_{xc}(\vec{r})$ is the exchange-correlation energy per electron of the PBE functional is calculated by expressing the electron density into local contributions $n_R(\vec{r})$ defined as

$$n_R(\vec{r}) = \sum_{ab \in R} \langle \vec{r}, \sigma | \chi_{R_a} \rangle \rho_{ab} \langle \chi_{R_a} | \vec{r}, \sigma \rangle. \tag{6}$$

The total density $n(\vec{r})$ in Eqn 5 is represented by the one-center expansion of the density, constructed using the partial waves used in the augmentation of the wave functions.[32]

Although this local approximation resembles DFT+U, the PBE0r functional treats all electrons equally without the need to selectively target specific orbital shells. The PBE0r functional also includes the exchange interaction between core and valence electrons. Another difference to the DFT+U method is form of the double-counting correction. In PBE0r the double counting correction subtracts the the local terms of the DFT exchange that correspond to the terms of the additional Fock term E_X^{HF}.[32] PBE0r accounts for on-site exchange interactions between atomic orbitals within the same atom. This interaction splits initially degenerate states into filled orbitals and empty orbitals. These bands are similar to the upper and lower Hubbard bands, with their separation approximately proportional to the Hubbard U value in DFT+U.

Recently, several range-separated hybrid functionals have been proposed[36,37] which show improvement over global hybrids in the prediction of band gaps, lattice parameters, and thermochemical properties.[38,39] The global hybrids tend to overestimate long-range exchange effects. The range-separated hybrid functionals split the exchange potential into short-range and long-range parts. The free parameters in these functionals are the range separation parameter ω and the HF mixing parameters in both the short- and long-range limits. The widely used HSE range-separated functional[36] incorporates 25% HF exchange exclusively for

the short-range part while the exchange interactions in the long-range part are treated at the PBE level. In HSE06,[37] the value of the range separation parameter ω is set to 0.11 bohr^{-1}. When $\omega = 0$, the HSE functional approaches PBE0. On the other hand, HSE becomes PBE for $\omega \to \infty$.

The range-separation and the screening of the Coulomb interactions in PBE0r functional is achieved by excluding the HF exchange matrix elements involving tight-binding orbital localized on different atoms. The cutoff of the exchange interaction depends on the spread of the localized tight-binding orbitals. The PBE0r results converge to HSE06, which includes exact HF exchange within the approximate 9 bohr radii, by going beyond the PBE0r's on-site approximation and incorporating HF-exchange terms that involve local orbitals centered on atoms linked by short distances, including nearest and next-nearest pairs. The PBE0r functional also has close similarity with the local hybrid functionals. In PBE0r, the HF exchange terms are partitioned into atomic contributions, which allows the optimization of each atom's exact exchange admixture. This is similar to the concept of local hybrid functionals, which incorporate a position-dependent admixture of the HF exchange through a local mixing function.

This study explores the efficacy of the local hybrid functional PBE0r in describing the spin crossover behavior for a large set consisting of Fe(II) complexes curated and studied by Vennelakanti et al.[26] with 23 DFAs, including B3LYP,[29,40,41] M06-L,[42] and TPSSh functionals.[43,44] In the original work, the set of 95 Fe(II) spin crossover complexes was curated by requiring that the structures had been isolated in both the low-spin and high-spin states, with high quality crystal structures available for both states. It also required that there be a discernible difference in the metal-ligand bond between the two spin states to ensure that a true spin transition had been captured. In addition, the $T_{1/2}$ was successfully recorded for the majority (i.e., 76 of 95 complexes) or approximated as the average of the temperature at which the low-spin and high-spin structures were crystallized. As a consequence of these curation criteria, these complexes feature mostly nitrogen-coordinating ligands with vary-

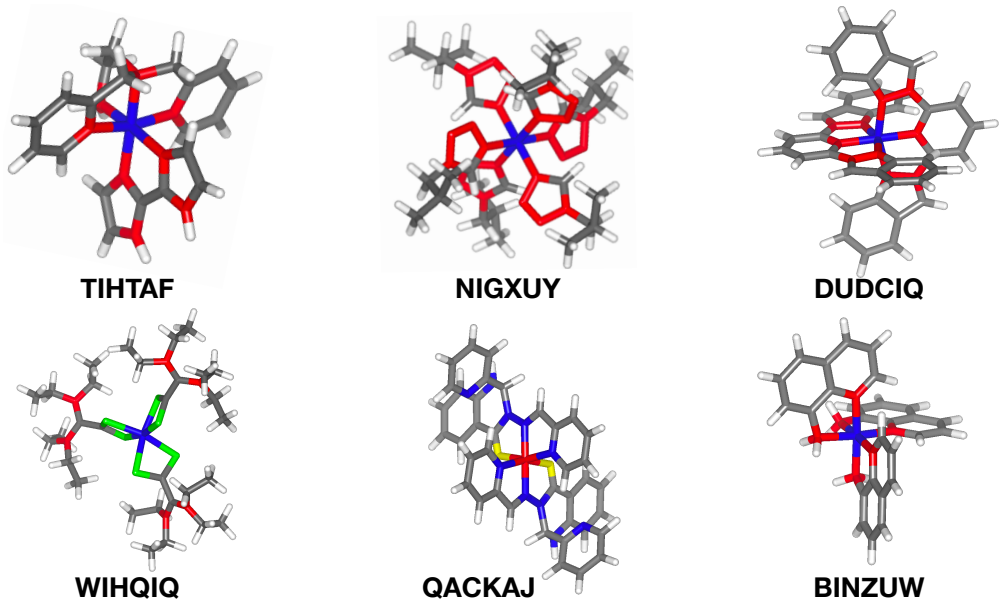

Figure 1: Representative examples of Fe(II) complexes from SCO-95 dataset studied in this work. Optimized geometry of all 95 complexes in HS as well as LS states, can be found in the Supplemental Material. Iron, nitrogen, carbon, hydrogen, sulfur, and oxygen are shown in blue, red, gray, white, green and yellow respectively.

ing denticity from monodentate to hexadentate. A small minority of complexes coordinate the metal with sulfur instead. Figure 1 displays representative examples of the complexes studied in the present work.

Calculation Setup

Calculations reported in this paper were performed within the DFT framework[45,46] using the projected augmented plane-wave method.[47] All calculations are carried out with the CP-PAW code.[48] The augmentation of the PAW method includes the 3d, 4s, 4p, orbitals on Fe, 1s orbital on H, the 2s, 2p, 3d orbitals on B, C, N, O, and F, the 3s, 3p, 3d orbitals on P, S, and Cl, and the 4s, 4p, 3d, 5s orbitals on Br, and the 4s, 3d, 4p orbitals on I. The auxiliary wave functions are expanded up to a plane-wave cutoff of 40 Ry, and the auxiliary density to a plane-wave cutoff of 80 Ry. The matching radii r_{cl}/r_{cov}, in units of covalent radius, used in the construction of partial waves are 0.90 for Fe, 1.20 for H, 0.95 for Br, 0.85 for B, C, I, and Cl, and 0.75 for N, O, S, and F. The tight-binding orbitals includes the 1s

orbital of H, the 2s and 2p orbitals of O, the 3d and 4s orbitals of Fe, the 2s and 2p orbitals of B, C, N, and F, the 3s and 3p orbitals of P, S, and Cl, the 4s, 4p, and 3d orbitals of Br, and the 4d, 5s, and 5p orbitals of I. The input setup file for these calculations is provided in the Supplemental Material. The calculations were performed using a periodic arrangement of Fe(II) complexes, employing a unit cell size that ensures a separation greater than 10 angstroms between periodic images of molecules. The long-range electrostatic interaction of periodic images is also removed, as detailed in reference.[49]

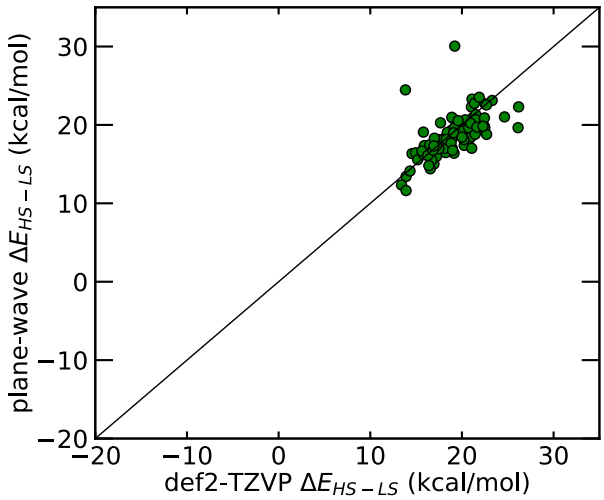

Figure 2: ΔE_{HS-LS} calculated for SCO complexes in SC0-95 data set with PBE/PW with frozen core approximation versus ΔE_{HS-LS} calculated with PBE/def2-TZVP//PBE/LACVP*.

Results and discussion

First, we look at the dependence of the calculated HS and LS state energy difference ΔE_{HS-LS}=E_{HS}−E_{LS} on the choice of the basis-set. Here, E_{HS} and E_{LS} represent the energy of the HS and LS states in their optimized geometries, respectively. The calculated ΔE_{HS-LS} values are sensitive to the parameters for the matching radius r_{cl}/r_{cov} of the Fe atom used in the construction of partial-waves. We determine suitable r_{cl}/r_{cov} values to ensure that the deviations in ΔE_{HS-LS} calculated from our plane-wave with frozen core

approximation compared to previous calculations[26] with def2-TZVP[50] for the PBE functional fall within the acceptable range of -3 to 3 kcal/mol. The PBE/def2-TZVP energies for SCO complexes are calculated using geometries optimized with the LACVP$*$ basis set, which includes an effective core potential for iron and heavier elements.[51,52] Full details of the calculations are provided in Vennelakanti et al.[26]

Figure 2 shows the parity plots of ΔE_{HS-LS} with the PBE functional between def2-TZVP (PBE/def2-TZVP//PBE/LACVP*) and the plane-wave (PBE/PW) basis sets. The spin splitting energies obtained with the PBE/PW with r_{cl}/r_{cov}=0.90 values for Fe-atom are consistently in good agreement with those obtained with PBE/def2-TZVP//PBE/LACVP*. Throughout this work, we use r_{cl}/r_{cov}=0.90 for the Fe atom.

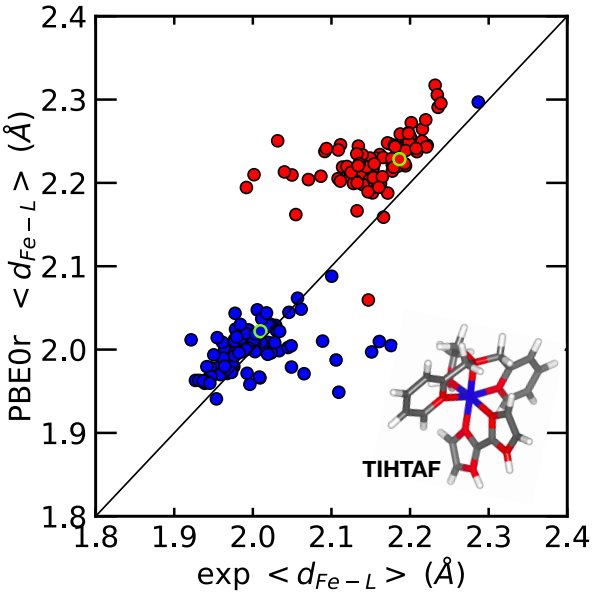

Figure 3: Experimental vs PBE0r Fe-ligands bond lengths for Fe(II) complexes in SCO-95. Red and blue circles indicate SCO complexes at high temperature with high-spin configuration and at low temperature with low-spin configuration, respectively. The solid black line is the parity line. A representative SCO complex with refcode: TIHTAF is shown in the inset. Hydrogen, carbon, nitrogen, and iron are shown in white, gray, red, and blue, respectively. Green circles denote the bond lengths for the representative SCO.

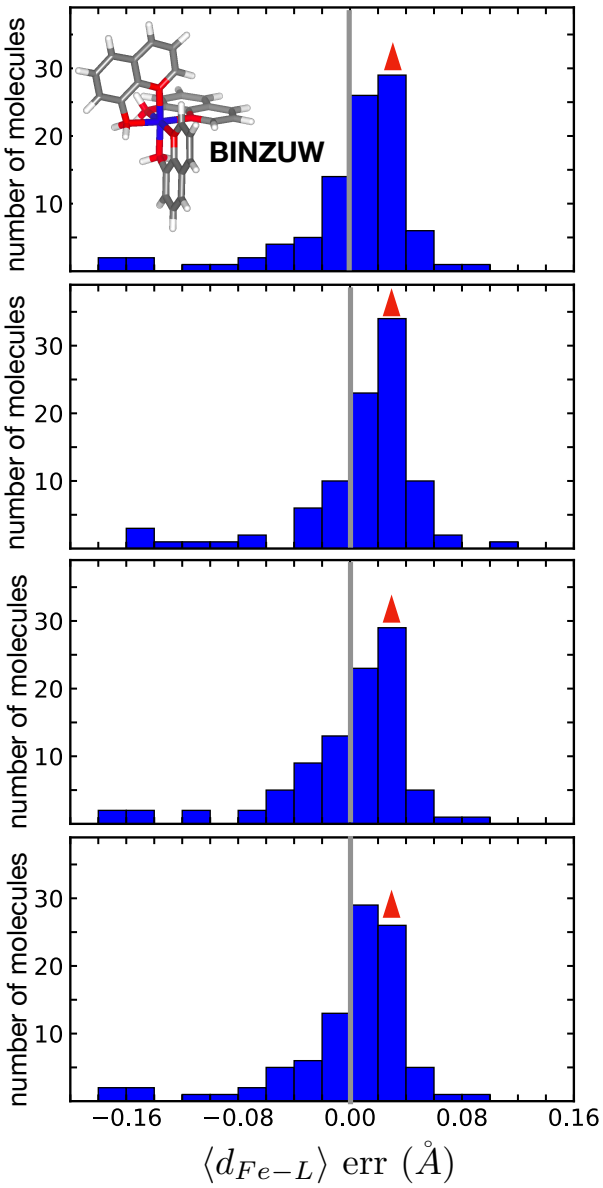

Figure 4: Histograms showing the distribution of average Fe–ligand bond length errors with with PBE and PBE0r, top to bottom: PBE, PBE0r (α=2.5%), PBE0r (α=4.0%) and PBE0r (α=7.5%). Bond length errors are computed between experimental low-temperature crystal structures and geometries optimized with PBE and PBE0r in the LS state. The bin-width in these plots is 0.02 Angstrom. The dashed vertical black line is the zero-axis. A representative SCO complex with refcode: BINZUW is shown in the inset. Hydrogen, carbon, nitrogen, and iron are shown in white, gray, red, and blue, respectively. A red triangle on top of a bar indicates the average Fe–ligand bond length errors of the inset complex.

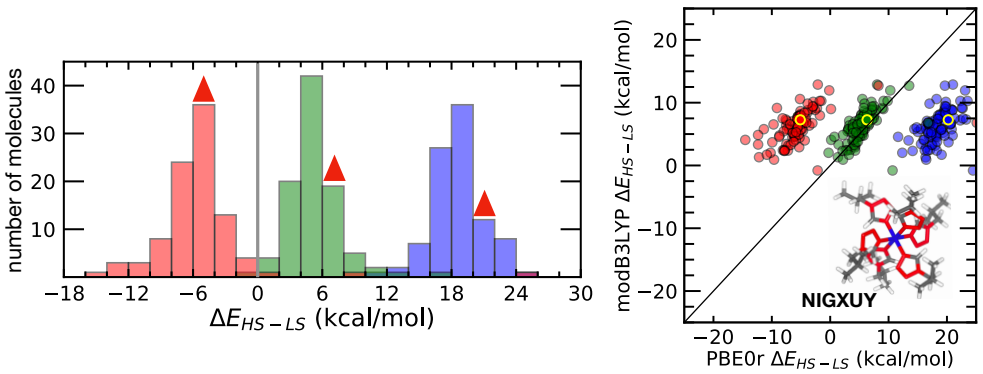

Figure 5: Left: Histograms showing the distribution of spin-splitting electronic energies ΔE_{HS-LS} calculated with PBE (blue) and PBE0r with the HF exchange factor α=4% (green) and α=7.5% (red). The gray vertical line represents the zero axis. The bin-width in these plots is 2.0 kcal/mol. Right: PBE and PBE0r versus modB3LYP (a_{HF}=10%) calculated ΔE_{HS-LS}. The blue solid circles indicate the PBE results and the green and red solid circles indicate the PBE0r results with the HF exchange α = 4.0 and 7.5 %, respectively. A representative SCO complex with refcode: NIGXUV is shown in the inset. Hydrogen, carbon, nitrogen, and iron are shown in white, gray, red, and blue, respectively. For the left pane, a red triangle above a bar indicates ΔE_{HS-LS} of the inset complex. For the right pane, yellow circles denote ΔE_{HS-LS} corresponding to the reference complex in the right inset.

Effect of Hartree-Fock exchange parameter α

We use LS and HS state geometries calculated with the PBE functional to carry out further structural optimizations using the local hybrid PBE0r for each Fe(II) complex in SCO-95. The energy convergence criterion is set to 1x10^{-6} Hartree. We examined the dependence of the geometries and spin-splitting energies ΔE_{HS-LS} of Fe(II) complexes in SCO-95 on the choice of the HF exchange factor α, which specifies the exact exchange weight in PBE0r, as discussed in the Method section. We keep the HF exchange mixing α the same for all atoms.

Figure 3 displays a comparison between metal-ligand bond lengths in PBE-optimized geometries and experimental high-T and low-T structures corresponding to the HS and LS states. Across these complexes, the experimental average Fe-metal bond lengths are consistently larger in the HS state, which is accurately predicted by PBE and PBE0r (α=2.5, 4.0, 5.0, 7.5 and 10%). The PBE and PBE0r bond lengths for both the LS and HS states are typically longer than their experimental bond lengths. There are noticeable differences

between the bond lengths predicted by PBE and those observed experimentally in complexes where the experimental average metal-ligand bond lengths are comparable in both low-temperature and high-temperature structures. This includes complexes represented by refcodes: VIFNAC, GETTEH, NIGXUY, EXARAY, and YUYHOR.

Figure 4 displays the metal-ligand bond length errors for the LS states for SCO-95. Here, the bond length error is defined as the difference between the predicted average Fe-ligand bond length $\langle d_{Fe-L} \rangle$ using PBE0r (where $\langle d_{Fe-L} \rangle = \sum_{i=1}^{6} d_{Fe-L_i}$ for octahedral Fe complexes) and the corresponding experimental average Fe-ligand bond length. The HF exchange factor α has very little effect on bond lengths. 67% of the complexes optimized using PBE display positive bond length errors, with similar percentages of approximately 75% and 63% observed for PBE0r-calculated complexes using HF exchange $\alpha = 4\%$ and 10%, respectively. These results contrast with earlier studies involving global hybrids, where delocalization errors, particularly in the LS states, indicated that the bond lengths were sensitive to the HF exchange.[26] The HF exchange terms in the PBE0r functional not only exclude the long-range exchange but also the offsite bond exchange, which involves the density of one site interacting with that at nearby sites. The absence of such exchange terms between the Fe atom and its ligands in PBE0r explains the reduced effect of the HF exchange factor α on the bond lengths in the LS states. This offsite exchange, present in the global and range-separated hybrid functional, affects the delocalized states with stronger covalent bonding, such as the LS states of Fe(II) complexes in this context.

Figure 5-left presents a comparison of ΔE_{HS-LS} values computed using PBE and PBE0r (α=4.0 and 7.5%) functionals. The positive ΔE_{HS-LS} values observed for all SCO complexes with both PBE and PBE0r (α=4.0%), except for one case with PBE0r, suggest that the LS states are more stabilized. However, the smaller ΔE_{HS-LS} values obtained with PBE0r (α=4.0%) indicate the reduced stability of the LS states compared to PBE. We also compared ΔE_{HS-LS} values from PBE0r at different α with those from a previous study using a modified version of the global hybrid B3LYP (modB3LYP) of the same SCO-95 dataset of Fe(II)

complexes. Previously, modB3LYP with a 10% HF exchange mixing was identified as the optimal choice for accurately predicting the SCO behavior across the majority of complexes in SCO-95. We observe that PBE0r with a 4.0% HF exchange ratio predicts a ΔE_{HS-LS} distribution that closely resembles the corresponding values predicted by modB3LYP with a 10% HF exchange. This optimum value of α is in line with the small HF exchange values found in earlier DFT studies of transition metal oxides and Fe(II) complexes employing the same PBE0r functional.[23,31,53]

With the exceptions of outliers WIHQIQ, ECODIM, and NIGXUY, the difference in ΔE_{HS-LS} predicted by modB3LYP (a_{HF}=10%) and PBE0r (α=4%) is less than 4.5 kcal/mol. We attempt to identify any common features among these complexes that may explain the observed differences in the calculated ΔE_{HS-LS} values. Notably, while ECODIM has two nitrogen atoms replaced with boron, WIHQIQ has three nitrogen atoms replaced with sulfur. The outlier NIGXUY is hexakis monodentate complexes.

Raising the HF exchange α in PBE0r further from α=4% to 5% results in 13% complexes exhibiting negative ΔE_{HS-LS} values, suggesting stabilization of the HS state for these complexes. With a 7.5% HF exchange, the PBE0r calculated ΔE_{HS-LS} values for all SCO-95 complexes, except WIHQIQ, become negative. This trend aligns with the findings of modB3LYP, which also demonstrated a preference for HS states with higher HF exchange ratios.[26]

Entropy contribution and Gibbs free energies

The role of entropy cannot be ignored in the spin transition of SCO systems at finite temperatures.[54–56] In Fe(II) complexes, similar electronic energies for different spin states trigger a thermally induced spin crossover. The HS state, which has longer metal-ligand bonds, tends to have a larger vibrational entropy.[57–59] This entropy effect becomes more prominent at higher temperatures and is largely responsible for the experimentally observed transition from LS to HS. We calculate the Gibbs free energies of the complexes in the SCO-95

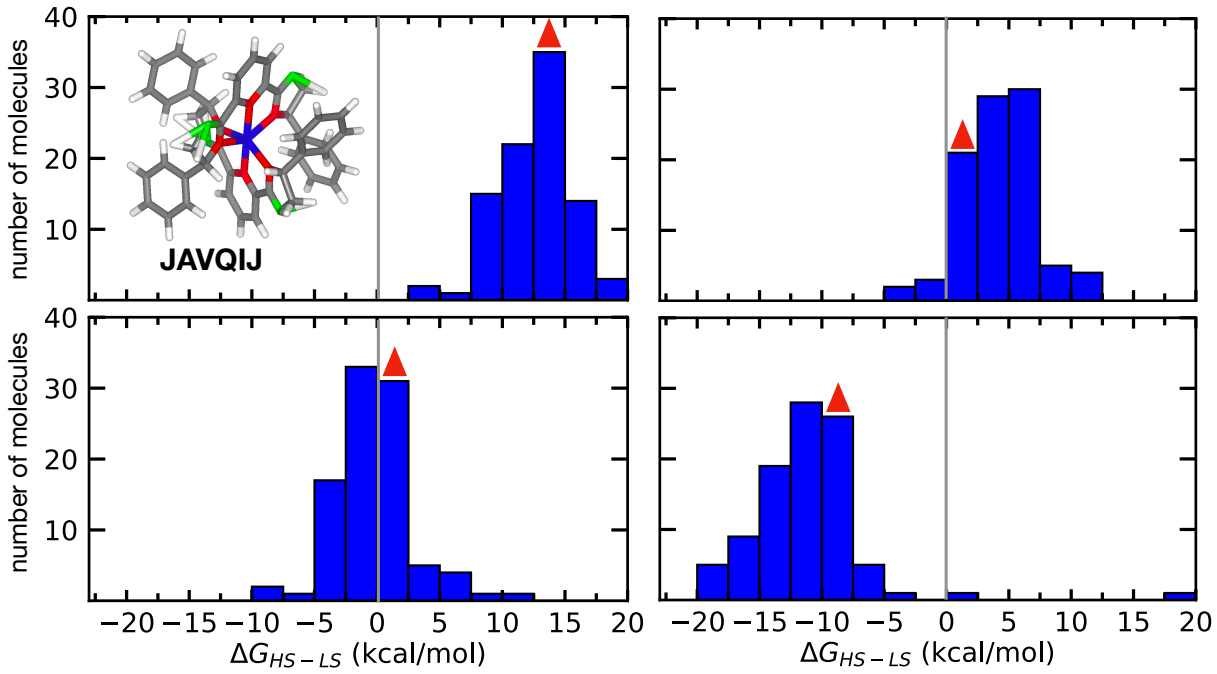

Figure 6: Histogram showing the distributing spin-splitting Gibbs free energies (ΔG_{HS-LS}) for 95 SCO complexes in SCO-95 with PBE ((top-left)) and PBE0r at different HF exchange α values from 2.5 % (top-right) to 4.0 %(bottom-left) and 7.5% (bottom-right) in the PBE0r functional. The bin-width in these plots is 2.5 kcal/mol. The solid gray vertical lines represent zero axes in all the plots. A representative SCO complex (refcode: JAVQIJ) is shown in the inset, and the bin that contains its property value is marked with a red star in each panel. Hydrogen, carbon, nitrogen, oxygen and iron are shown in white, gray, red, green, and blue, respectively.

dataset to investigate the efficacy of the PBE0r functional in describing the SCO behavior. To determine the free energies, we use the zero-point energy and entropic contributions (i.e., electronic, rotational, and vibrational components) obtained with T=300 K using the modB3LYP functional and LACVP* basis-set from the previous study on isolated gas phase molecules.[26] For electronic entropy, a constant configurational electronic entropy contribution of 0.9595 kcal/mol is considered for high-spin states (S=2) of Fe(II) complexes within SCO-95, where the degeneracy is 2S+1=5. Since the average thermodynamic corrections to free energy are found to be consistently similar in reference[26] across all a_{HF} values, we only use the free energy corrections calculated with modB3LYP with $a_{HF} = 10\%$.

Figure 6 illustrates how the free energy difference ΔG_{HS-LS} varies when calculated using PBE and PBE0r with different HF exchange: α= 0, 4.0, and 7.5%. Incorporating the entropy term $T\Delta S$ into the spin-splitting energy differences ΔE_{HS-LS} calculated from pure PBE and PBE0r with a small HF exchange (α=2.5%) continues to favor the LS states. This preference is evident in the positive free energies ΔG_{HS-LS} for all complexes under PBE and 94% of complexes under PBE0r (α=2.5%). As α increases, the positive values of ΔG_{HS-LS} decrease, indicating a reduced stability of the LS states. Slightly negative values for free energy changes ΔG_{HS-LS} are observed for 6% of complexes already at small HF exchange α=2.5%. As α reaches 7.5%, all but two SCO complexes exhibit negative ΔG_{HS-LS} values, suggesting that the free energy favors the HS states. The PBE0r calculated ΔG_{HS-LS} values for the SCOs consistently show a few outliers (refcodes: WIHQIQ, QAXQIR, YAGYUB, SESNEM, WEXVON and ZERDOS, UXOHEW GOGSAZ, and LAGJEK) across all HF exchange factors α. Among these, SESNEM, LAGJEK and YAGYUB display a slightly stronger preference for HS states, while the complexes WIHQIQ, WEXVON, UXOHEW, ZERDOS, GOGSAZ and QAXQIR lean towards LS states.

The PBE0r functional with α=4% predicts ΔG_{HS-LS} values predominantly falling within the range of -5.5 to 5.5 kcal/mol, suggested as an optimal range to describe the SCO behavior in previous studies on the same SCO-95 dataset. The PBE0r with α=4% predicts ΔG_{HS-LS}

of 90% of SCO-95 complexes within this ideal range. The complexes that are not predicted to be SCO complexes are WIHQIQ, QAXQIR, YAGYUB, SESNEM, WEXVON, and ZERDOS, UXOHEW GOGSAZ, and LAGJEK. With a slightly higher α=5%, a smaller fraction, 74%, of complexes have their ΔG_{HS-LS} values predicted within the optimal range of -5.5 to 5.5 kcal/mol.

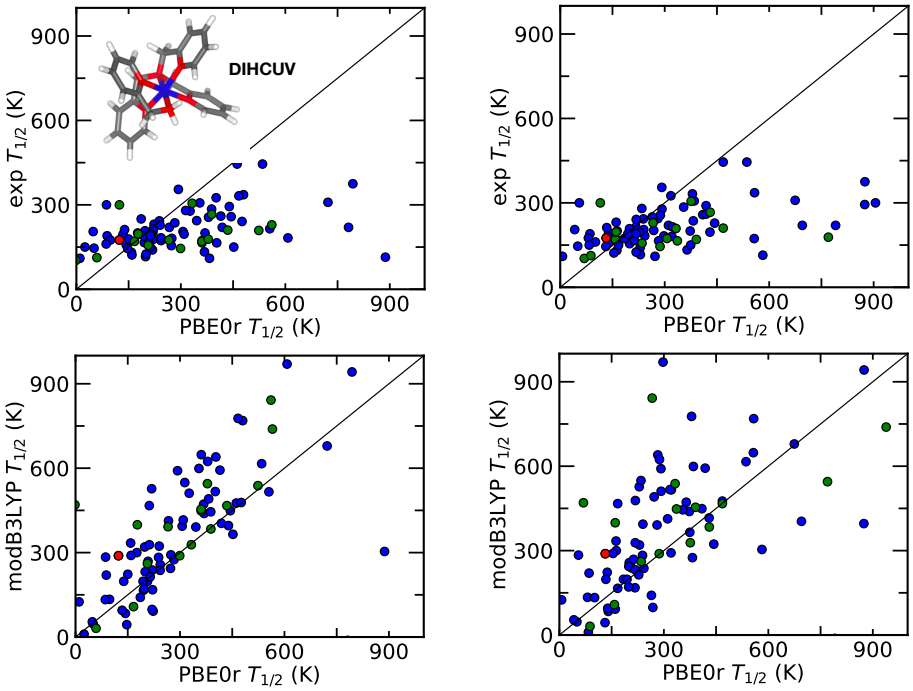

Figure 7: Top: Comparison between the experimental SCO transition temperature $T_{1/2}$ and PBE0r predicted $T_{1/2}$ for 95 complexes in the SCO-95 database. Bottom: Deviation between modB3LYP and PBE0r predicted $T_{1/2}$ values for the same SCO dataset. In both left panels, PBE0r $T_{1/2}$ estimated values utilize thermodynamic corrections obtained from modB3LYP ($a_{HF} = 0\%$), while the right panels use thermodynamic corrections with modB3LYP ($a_{HF} = 10\%$). The blue symbols represent 76 complexes from the SCO-95 dataset with available experimental $T_{1/2}$ exhibiting reported single-step SCO behavior. The green symbols denote the remaining 18 complexes, where we consider their experimental $T_{1/2}$ as the average of experimental low-temperature and high-temperature crystallization values. Solid black lines depict the parity lines. The red symbol highlights the $T_{1/2}$ values for a representative Fe(II) complex with refcode: DIHCUV which is shown in the inset of the top-left. Hydrogen, carbon, nitrogen, and iron atoms are depicted in white, gray, red, and blue, respectively.

Estimated spin crossover transition temperature $T_{1/2}$

We determine the theoretical spin crossover temperature, denoted as $T_{1/2}$, for all complexes in SCO-95 using PBE0r. This relies on identifying the temperature at which the Gibbs free energies of the HS and LS states are the same. This relationship is expressed as $T_{1/2} = \Delta H_{HS-LS}/\Delta S_{HS-LS}$. The entropy corrections for the spin states of each complex were obtained from thermodynamic calculations at T=300 K. Here, we assumed that the temperature dependence of these entropic corrections was negligible. We used the zero-point energy, the thermal vibrational energy (electronic, rotational, and vibrational), and the entropic contribution obtained with the modB3LYP at 10% HF exchange from the previous study[26] to estimate the $T_{1/2}$ values.

The SCO transition temperatures $T_{1/2}$ for majority of complexes predicted from PBE0r tends to be out of range of the experimentally reported SCO transition temperature if the calculated values ΔG_{HS-LS} are not within -5 to 5 kcal/mol. The PBE0r with α=4% predicts $T_{1/2}$ that fall largely within the range of experimentally reported $T_{1/2}$ of 0 to 450 K. In Figure 7-top, we present a comparison between PBE0r predicted $T_{1/2}$ and experimental $T_{1/2}$. The experimental $T_{1/2}$ is available for 76 complexes with reported single-step SCO behavior reported in the SCO-95 dataset. For the remaining 18 complexes in the SCO-95 dataset where $T_{1/2}$ is not available or a two-step SCO behavior is reported, we consider the average of experimental low-temperature and high-temperature crystallization values.

The PBE0r predicted $T_{1/2}$ distribution using thermodynamic corrections obtained from modBPLYP with different HF exchange a_{HF}=0% and a_{HF}=10% remain largely similar. The $T_{1/2}$ predictions from PBE0r (α= 4%) with modBPLYP(a_{HF} = 10%) thermodynamic corrections of 79% complexes fall within 0-450 K. Outlier systems include five complexes with negative $T_{1/2}$ (refcode: DUBFOY, ECODIM, SESNEM, JIQDET and NALPIB) and 16 complexes with $T_{1/2}$>450. The negative $T_{1/2}$ estimated for ECODIM can be attributed to its negative entropic spin-splitting energies ΔS_{HS-LS}, while the negative enthalpy changes predicted for the others explain their predicted negative $T_{1/2}$. Of the 18 complexes with

PBE0r estimated $T_{1/2}$>450, ZERDOS, WIHQIQ, WEXVON, and QAXQIR have notably large positive changes in enthalpy.

The PBE0r functional shows improved performance with approximately 78% of its predicted $T_{1/2}$ values falling within the experimental $T_{1/2}$ range 0-450 K, compared to 63% for modB3LYP (with $a_{HF} = 10\%$). The outliers ECODOS, NALPIB, QAXQIR, WEXVON WIHQIQ, and UXOHEW stand out due to the significant gaps between their experimentally observed $T_{1/2}$ values and those predicted by PBE0r.

In the lower panels of Figure 7, the predicted $T_{1/2}$ of modB3LYP is compared to the $T_{1/2}$ calculated using PBE0r. The PBE0r calculations of $T_{1/2}$ uses thermodynamic corrections with modBPLYP at $a_{HF} = 0\%$ and 10% from the earlier study by Vennelakanti et al.[26] Unlike the spin-splitting energies ΔE_{HS-LS} and ΔG_{HS-LS}, the SCO transition temperatures estimated with PBE0r and modB3LYP do not exhibit a strong correlation. "The PBE0r $T_{1/2}$ values calculated using thermodynamic corrections estimated with modB3LYP ($a_{HF} = 10\%$) show a stronger correlation with modB3LYP (with a_{HF}=10%) $T_{1/2}$ values, compared to those calculated using thermodynamic corrections with modB3LYP ($a_{HF} = 0\%$). The prior investigation on SCO-95 with modB3LYP highlights a significant dependence on the predicted $T_{1/2}$ values on the vibrational entropies. Instead of explicit PBE0r calculated thermodynamic corrections, using the thermodynamic contributions computed with modB3LYP for estimating $T_{1/2}$ by PBE0r in our present study may contribute to the deviation observed between the predicted $T_{1/2}$ values.

Conclusions

This work studied an extensive set of 95 different iron SCO complexes with local hybrid functional PBE0r. This same set of SCO complexes was previously studied using the modified B3LYP functional with varying HF exchange fractions and 23 other density functional approximations, including TPSSh and M06-L. Overall, the PBE0r predictions of $T_{1/2}$ are

largely consistent with modBPLYP with a few outliers. Our results for both electronic ΔE_{HS-LS} and Gibbs free ΔG_{HS-LS} spin-splitting energies predicted with different HF exchange factors α are consistent with the previous calculation that indicates an overall change in the preferred ground state from LS to HS with an increasing fraction of HF exchange in the modB3LYP functional. Although the predictions of the SCO transition temperatures $T_{1/2}$ by PBE0r with an HF exchange mixing factor of $\alpha = 4\%$ are consistent with modB3LYP, they have limitations in accurately reflecting experimental $T_{1/2}$ trends.

Supplemental Information

The supplemental information contain the following: optimized geometries of SCO in both high-spin (HS) and low-spin (LS) states, predicted transition temperatures, example input setup files used for optimizing electronic structure and geometries with PBE0r, and the predicted electronic energies and Gibbs free spin-splitting energies.

Acknowledgment

This work was primarily supported by the U.S. Department of Energy, Office of Science, Basic Energy Sciences, Materials Sciences, and Engineering Division, as part of the Computational Materials Sciences Program. H.J.K. was supported by a Alfred P. Sloan Fellowship in Chemistry, a Simon Faculty Research Innovation Fund, and the U.S. Department of Energy under Grant number DE-SC0024174.

References

(1) Bousseksou, A.; Molnár, G.; Salmon, L.; Nicolazzi, W. Molecular spin crossover phenomenon: recent achievements and prospects. *Chem. Soc. Rev.* **2011**, *40*, 3313–3335.

(2) Brooker, S. Spin crossover with thermal hysteresis: practicalities and lessons learnt. *Chem. Soc. Rev.* **2015**, *44*, 2880–2892.

(3) Molnár, G.; Salmon, L.; Nicolazzi, W.; Terki, F.; Bousseksou, A. Emerging properties and applications of spin crossover nanomaterials. *J. Mater. Chem. C* **2014**, *2*, 1360–1366.

(4) Gütlich, P.; Garcia, Y.; Goodwin, H. A. Spin crossover phenomena in Fe() complexes. *Chem. Soc. Rev.* **2000**, *29*, 419–427.

(5) Real, J. A.; Gaspar, A. B.; Muñoz, M. C. Thermal, pressure and light switchable spin-crossover materials. *Dalton Trans.* **2005**, 2062–2079.

(6) Raghavachari, K.; Trucks, G. W.; Pople, J. A.; Head-Gordon, M. A fifth-order perturbation comparison of electron correlation theories. *Chemical Physics Letters* **1989**, *157*, 479–483.

(7) Andersson, K.; Malmqvist, P. A.; Roos, B. O.; Sadlej, A. J.; Wolinski, K. Second-order perturbation theory with a CASSCF reference function. *The Journal of Physical Chemistry* **1990**, *94*, 5483–5488.

(8) Andersson, K.; Malmqvist, P.-Å.; Roos, B. O. Second-order perturbation theory with a complete active space self-consistent field reference function. **1992**, *96*, 1218–1226.

(9) Radoń, M.; Broclawik, E.; Pierloot, K. DFT and Ab Initio Study of Iron-Oxo Porphyrins: May They Have a Low-Lying Iron(V)-Oxo Electromer? *Journal of Chemical Theory and Computation* **2011**, *7*, 898–908.

(10) Radoń, M. Benchmarking quantum chemistry methods for spin-state energetics of iron complexes against quantitative experimental data. *Phys. Chem. Chem. Phys.* **2019**, *21*, 4854–4870.

(11) Neese, F.; Wennmohs, F.; Hansen, A. Efficient and accurate local approximations to coupled-electron pair approaches: An attempt to revive the pair natural orbital method. *The Journal of Chemical Physics* **2009**, *130*, 114108.

(12) Riplinger, C.; Neese, F. An efficient and near linear scaling pair natural orbital based local coupled cluster method. *The Journal of Chemical Physics* **2013**, *138*, 034106.

(13) Riplinger, C.; Sandhoefer, B.; Hansen, A.; Neese, F. Natural triple excitations in local coupled cluster calculations with pair natural orbitals. *The Journal of Chemical Physics* **2013**, *139*, 134101.

(14) Riplinger, C.; Pinski, P.; Becker, U.; Valeev, E. F.; Neese, F. Sparse maps—A systematic infrastructure for reduced-scaling electronic structure methods. II. Linear scaling domain based pair natural orbital coupled cluster theory. *The Journal of Chemical Physics* **2016**, *144*, 024109.

(15) Sparta, M.; Neese, F. Chemical applications carried out by local pair natural orbital based coupled-cluster methods. *Chem. Soc. Rev.* **2014**, *43*, 5032–5041.

(16) Saitow, M.; Neese, F. Accurate spin-densities based on the domain-based local pair-natural orbital coupled-cluster theory. *The Journal of Chemical Physics* **2018**, *149*, 034104.

(17) Vancoillie, S.; Zhao, H.; Radoń, M.; Pierloot, K. Performance of CASPT2 and DFT for Relative Spin-State Energetics of Heme Models. *Journal of Chemical Theory and Computation* **2010**, *6*, 576–582.

(18) Pierloot, K.; Phung, Q. M.; Domingo, A. Spin State Energetics in First-Row Transition Metal Complexes: Contribution of (3s3p) Correlation and Its Description by Second-Order Perturbation Theory. *Journal of Chemical Theory and Computation* **2017**, *13*, 537–553.

(19) Phung, Q. M.; Feldt, M.; Harvey, J. N.; Pierloot, K. Toward Highly Accurate Spin State Energetics in First-Row Transition Metal Complexes: A Combined CASPT2/CC Approach. *Journal of Chemical Theory and Computation* **2018**, *14*, 2446–2455.

(20) Reiher, M.; Salomon, O.; Artur Hess, B. Reparameterization of hybrid functionals based on energy differences of states of different multiplicity. *Theoretical Chemistry Accounts* **2001**, *107*, 48–55.

(21) Deeth, R. J.; Fey, N. The performance of nonhybrid density functionals for calculating the structures and spin states of Fe(II) and Fe(III) complexes. *Journal of Computational Chemistry* **2004**, *25*, 1840–1848.

(22) Swart, M.; Groenhof, A.; Ehlers, A. W.; Lammertsma, K. Validation of ExchangeCorrelation Functionals for Spin States of Iron Complexes. *The Journal of Physical Chemistry A* **2004**, *108*, 5479–5483.

(23) Römer, A.; Hasecke, L.; Blöchl, P.; Mata, R. A. A Review of Density Functional Models for the Description of Fe(II) Spin-Crossover Complexes. *Molecules* **2020**, *25*.

(24) Verma, P.; Varga, Z.; Klein, J. E. M. N.; Cramer, C. J.; Que, L.; Truhlar, D. G. Assessment of electronic structure methods for the determination of the ground spin states of Fe(ii), Fe(iii) and Fe(iv) complexes. *Phys. Chem. Chem. Phys.* **2017**, *19*, 13049–13069.

(25) Droghetti, A.; Alfè, D.; Sanvito, S. Assessment of density functional theory for iron(II) molecules across the spin-crossover transition. *The Journal of Chemical Physics* **2012**, *137*, 124303.

(26) Vennelakanti, V.; Taylor, M. G.; Nandy, A.; Duan, C.; Kulik, H. J. Assessing the performance of approximate density functional theory on 95 experimentally characterized Fe(II) spin crossover complexes. *The Journal of Chemical Physics* **2023**, *159*, 024120.

(27) Cirera, J.; Via-Nadal, M.; Ruiz, E. Benchmarking Density Functional Methods for Calculation of State Energies of First Row Spin-Crossover Molecules. *Inorganic Chemistry* **2018**, *57*, 14097–14105.

(28) Adamo, C.; Barone, V. Toward reliable density functional methods without adjustable parameters: The PBE0 model. **1999**, *110*, 6158–6170.

(29) Becke, A. D. Density-functional thermochemistry. III. The role of exact exchange. **1993**, *98*, 5648–5652.

(30) Yanai, T.; Tew, D. P.; Handy, N. C. A new hybrid exchange–correlation functional using the Coulomb-attenuating method (CAM-B3LYP). *Chemical Physics Letters* **2004**, *393*, 51–57.

(31) Sotoudeh, M.; Rajpurohit, S.; Blöchl, P.; Mierwaldt, D.; Norpoth, J.; Roddatis, V.; Mildner, S.; Kressdorf, B.; Ifland, B.; Jooss, C. Electronic structure of $Pr_{1-x}Ca_xMnO_3$. *Phys. Rev. B* **2017**, *95*, 235150.

(32) Blöchl, P. E.; Walther, C. F. J.; Pruschke, T. Method to include explicit correlations into density-functional calculations based on density-matrix functional theory. **2011**, *84*, 205101.

(33) Blöchl, P. E.; Pruschke, T.; Potthoff, M. Density-matrix functionals from Green's functions. *Phys. Rev. B* **2013**, *88*, 205139.

(34) Perdew, J. P.; Burke, K.; Ernzerhof, M. Generalized Gradient Approximation Made Simple. *Phys. Rev. Lett.* **1996**, *77*, 3865–3868.

(35) Blöchl, P. E.; Först, C. Node-less atomic wave functions, Pauli repulsion and systematic projector augmentation. *arXiv* **2012**, *1210.5937*.

(36) Heyd, J.; Scuseria, G. E.; Ernzerhof, M. Hybrid functionals based on a screened Coulomb potential. *The Journal of Chemical Physics* **2003**, *118*, 8207–8215.

(37) Krukau, A. V.; Vydrov, O. A.; Izmaylov, A. F.; Scuseria, G. E. Influence of the exchange screening parameter on the performance of screened hybrid functionals. *The Journal of Chemical Physics* **2006**, *125*, 224106.

(38) Vydrov, O. A.; Heyd, J.; Krukau, A. V.; Scuseria, G. E. Importance of short-range versus long-range Hartree-Fock exchange for the performance of hybrid density functionals. *The Journal of Chemical Physics* **2006**, *125*, 074106.

(39) Ghose, K. K.; Brown, J. J.; Frankcombe, T. J.; Page, A.; Bayon, A. Density functional theory modeling of critical properties of perovskite oxides for water splitting applications. *WIREs Energy and Environment* **2023**, *12*, e476.

(40) Vosko, S. H.; Wilk, L.; Nusair, M. Accurate spin-dependent electron liquid correlation energies for local spin density calculations: a critical analysis. *Canadian Journal of Physics* **1980**, *59*, 1200.

(41) Lee, C.; Yang, W.; Parr, R. G. Development of the Colle-Salvetti correlation-energy formula into a functional of the electron density. *Phys. Rev. B* **1988**, *37*, 785–789.

(42) Zhao, Y.; Truhlar, D. G. A new local density functional for main-group thermochemistry, transition metal bonding, thermochemical kinetics, and noncovalent interactions. *The Journal of Chemical Physics* **2006**, *125*, 194101.

(43) Staroverov, V. N.; Scuseria, G. E.; Tao, J.; Perdew, J. P. Comparative assessment of a new nonempirical density functional: Molecules and hydrogen-bonded complexes. *The Journal of Chemical Physics* **2003**, *119*, 12129–12137.

(44) Tao, J.; Perdew, J. P.; Staroverov, V. N.; Scuseria, G. E. Climbing the Density Functional Ladder: Nonempirical Meta–Generalized Gradient Approximation Designed for Molecules and Solids. *Phys. Rev. Lett.* **2003**, *91*, 146401.

(45) Kohn, W.; Sham, L. J. Self-Consistent Equations Including Exchange and Correlation Effects. *Phys. Rev.* **1965**, *140*, A1133–A1138.

(46) Hohenberg, P.; Kohn, W. Inhomogeneous Electron Gas. *Phys. Rev.* **1964**, *136*, B864–B871.

(47) Blöchl, P. E. Projector augmented-wave method. *Phys. Rev. B* **1994**, *50*, 17953–17979.

(48) CP-PAW code. `https://cppaw.org/doku.php?id=start`.

(49) Blöchl, P. E. Electrostatic decoupling of periodic images of plane-wave-expanded densities and derived atomic point charges. *The Journal of Chemical Physics* **1995**, *103*, 7422–7428.

(50) Weigend, F.; Ahlrichs, R. Balanced basis sets of split valence, triple zeta valence and quadruple zeta valence quality for H to Rn: Design and assessment of accuracy. *Phys. Chem. Chem. Phys.* **2005**, *7*, 3297–3305.

(51) Hay, P. J.; Wadt, W. R. Ab initio effective core potentials for molecular calculations. Potentials for K to Au including the outermost core orbitals. **1985**, *82*, 299–310.

(52) Ditchfield, R.; Hehre, W. J.; Pople, J. A. Self-Consistent Molecular-Orbital Methods. IX. An Extended Gaussian-Type Basis for Molecular-Orbital Studies of Organic Molecules. *The Journal of Chemical Physics* **1971**, *54*, 724–728.

(53) Eckhoff, M.; Blöchl, P. E.; Behler, J. Hybrid density functional theory benchmark study on lithium manganese oxides. *Phys. Rev. B* **2020**, *101*, 205113.

(54) Sorai, M.; Seki, S. Phonon coupled cooperative low-spin 1A1high-spin 5T2 transition in [Fe(phen)2(NCS)2] and [Fe(phen)2(NCSe)2] crystals. *Journal of Physics and Chemistry of Solids* **1974**, *35*, 555–570.

(55) Gütlich, P.; Gaspar, A. B.; Garcia, Y. Spin state switching in iron coordination compounds. *Beilstein Journal of Organic Chemistry* **2013**, *9*.

(56) Kepp, K. P. Theoretical Study of Spin Crossover in 30 Iron Complexes. *Inorganic Chemistry* **2016**, *55*, 2717–2727.

(57) Brehm, G.; Reiher, M.; Schneider, S. Estimation of the Vibrational Contribution to the Entropy Change Associated with the Low- to High-Spin Transition in Fe(phen)2(NCS)2 Complexes: Results Obtained by IR and Raman Spectroscopy and DFT Calculations. *The Journal of Physical Chemistry A* **2002**, *106*, 12024–12034.

(58) Ronayne, K. L.; Paulsen, H.; Höfer, A.; Dennis, A. C.; Wolny, J. A.; Chumakov, A. I.; Schünemann, V.; Winkler, H.; Spiering, H.; Bousseksou, A.; Gütlich, P.; Trautwein, A. X.; McGarvey, J. J. Vibrational spectrum of the spin crossover complex [Fe(phen)2(NCS)2] studied by IR and Raman spectroscopy, nuclear inelastic scattering and DFT calculations. *Phys. Chem. Chem. Phys.* **2006**, *8*, 4685–4693.

(59) Density functional theory calculations and vibrational spectroscopy on iron spin-crossover compounds. *Coordination Chemistry Reviews* **2009**, *253*, 2423–2431, Deutsche Forschungsgemeinschaft Molecular Magnetism Research Report.

TOC Graphic

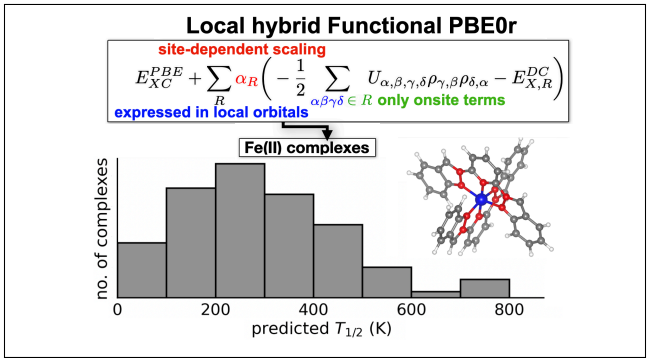
Local hybrid Functional PBE0r
site-dependent scaling
$E_{XC}^{PBE} + \sum_R \alpha_R \left(-\frac{1}{2} \sum_{\alpha\beta\gamma\delta \in R} U_{\alpha,\beta,\gamma,\delta} \rho_{\gamma,\beta} \rho_{\delta,\alpha} - E_{X,R}^{DC} \right)$
only onsite terms
expressed in local orbitals
Fe(II) complexes
no. of complexes
0
200
400
600
800
predicted $T_{1/2}$ (K)